

Stress Intensity Measurement via Infrared Focal Plane Array

Stress Photonics, Inc.

Jon R. Lesniak

Daniel J. Bazile

Bradley R. Boyce

Michael J. Zickel

NASA Langley Research Center

K. Elliott Cramer

College of William & Mary

Christopher S. Welch

Stress Photonics, Inc.
565 Science Dr.
Madison WI 53711

1.0 Introduction

There are many tools available that can monitor crack length in the laboratory including microscopes, potential drop, and crack mouth opening techniques. These measurements combined with analytical solutions, can be used to infer stress intensity factors and crack lengths. However, these approaches may not be as applicable to real components as they are to test coupons. This paper illustrates that Thermoelastic Stress Analysis (TSA) can be as powerful a tool in materials laboratories as it has been consistently demonstrated to be in component test facilities. TSA is a full-field measurement technique that shows great promise for measuring stress intensity factors on arbitrary structures. This paper describes recent progress in the measurement of mixed mode stress intensity factors of monolithic materials. The results are compared with analytical solutions of predetermined mode I and mixed mode I and II geometries. The solutions used in this application are intentionally general and are intended to demonstrate the methodology of the damage assessment system. Of course, no analysis is a perfect match for every situation, each user of this technology will have a unique set of concerns, but the layout of the thermoelastic damage assessment system accommodates improvements as well as facilitates further evolution of the technology into field applications, composite damage, test control, hostile environment testing and more.

2.0 Thermoelastic Primer

Thermoelastic Stress Analysis (TSA) is a full-field, non-contacting stress-analysis technique. An infrared array camera is used to measure small, load-induced temperature changes (ΔT) described by

$$\Delta T = -\frac{T}{C_p} (\alpha_x \sigma_x + \alpha_y \sigma_y) \quad (1)$$

where ρ is the density, α is the thermal expansion coefficient, C_p is the specific heat, T is the absolute temperature and σ_x and σ_y are the normal stress components. To improve measurements, the temperature changes induced by the thermoelastic effect are repeated and time-averaged with continuous dynamic loading. Although sinusoidal loading is most common, more complex load histories like those induced by traffic on a bridge can be used. Figure 1 is a block diagram of a typical laboratory setup. A closed-loop hydraulic load frame provides the loading while a TSA system correlates the load-induced IR signals with the reference signal from the load cell or strain gage. Because the cameras employed in TSA measure the amplitude of the temperature oscillation, not just the absolute temperature; they are referred to as differential thermographic cameras. Most often the differential thermographic camera operates in a lock-in mode, providing in-phase and out-of-phase images. When properly adjusted, the stress map resides in the in-phase image and the out-of-phase image is null.

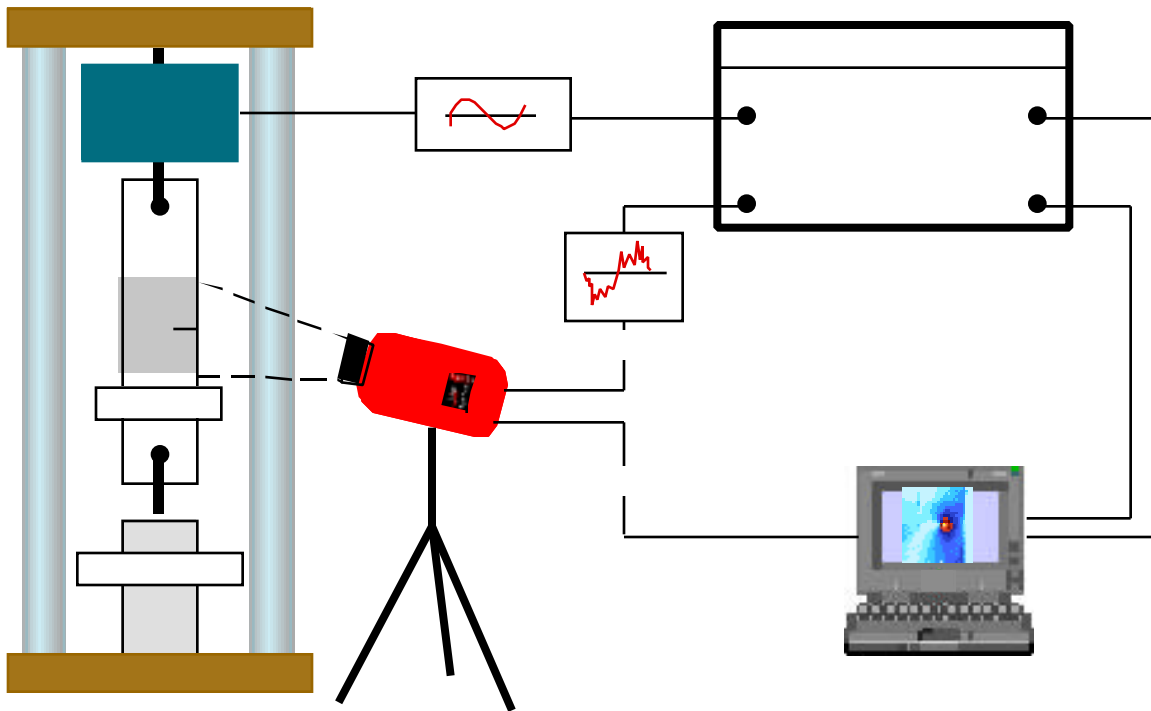


Fig. 1 TSA system block diagram.

3.0 Linear Elastic Stress Functions

In classical fracture mechanics, equations describing the stress singularity at the tip of a crack are often derived. However, because it is only the singular terms that drive failure or crack propagation the arguments rarely yield a complete solution for the stress distribution away from the crack tip. In order to measure stress intensity factors on arbitrary geometries using full field data, a general solution to all potential stress distributions must be sought.

To accomplish this solution a stress function approach is taken. In review, a plane elastic stress function in the presence of no body forces is a function that satisfies the biharmonic equation. This relation is derived considering the two equations of equilibrium as well as the stress compatibility equation. In polar coordinates the biharmonic equation is written

$$\nabla^4 (\phi, \psi) = \frac{\partial^2}{\partial r^2} + \frac{1}{r} \frac{\partial}{\partial r} + \frac{1}{r^2} \frac{\partial^2}{\partial \theta^2} \left(\frac{\partial^2}{\partial r^2} + \frac{1}{r} \frac{\partial}{\partial r} + \frac{1}{r^2} \frac{\partial^2}{\partial \theta^2} \right) = 0 \quad (2)$$

where ϕ is the stress function. Of course, the stress function does not describe the state of stress directly, rather the exact state of stress can be derived via the following differential operations

$$r = \frac{1}{r} + \frac{1}{r^2} \quad (3a)$$

$$= \frac{2}{r^2} \quad (3b)$$

$$= \frac{1}{r^2} - \frac{1}{r} \quad (3c)$$

It is important to note that the above defined stress distributions are valid for any plane-elastic case including plane strain and plane stress. For the zero body force problem it is not until strains must be calculated that conversion from one to the other is necessary.

Williams summarized the derivation of the stress functions of cracks[1]. The process is revisited here as several typographical errors in the Williams paper need to be clarified. The generic stress function for a notch with stress free edges is of the form

$$(r, \theta) = r^{n+1} [c_1 \sin(\theta + 1) + c_2 \cos(\theta + 1) + c_3 \sin(\theta - 1) + c_4 \cos(\theta - 1)] \quad (4)$$

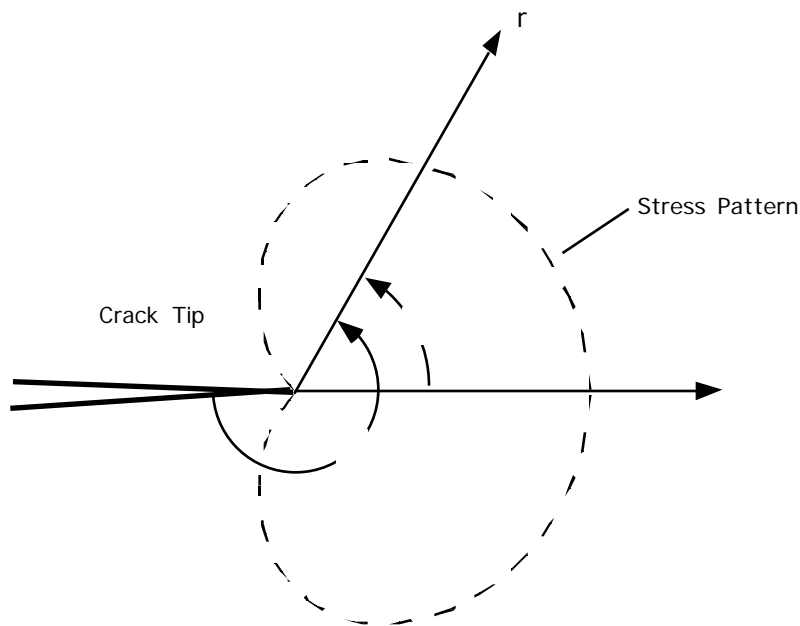


Fig. 2 Fracture mechanics coordinate system

where θ is defined in Fig. 2. The values of θ are described by the eigenequation

$$\sin(\theta) = \pm \sin \quad (5)$$

where θ is the angle subtended from edge to edge, which for a closed crack, $\theta = 2\pi$, yields

$$\theta = n/2 \quad \text{where } n=1,2,3,4 \dots \quad (6)$$

The generic stress function for a closed crack becomes

$$(r, \theta, n) = r^{n/2+1} [c_1 \sin(n\theta/2 + 1) + c_2 \cos(n\theta/2 + 1) + c_3 \sin(n\theta/2 - 1) + c_4 \cos(n\theta/2 - 1)] \quad (7)$$

The enforcement of boundary conditions at the free edges of the crack requires that,

$$= r^{n/2-1} [(n/2)(n/2 + 1)F(\theta, n)] = 0 \quad \text{For } \theta = 0, 2\pi \quad (8a)$$

$$r = r^{n/2-1} [-(n/2)F'(\theta, n)] = 0 \quad \text{For } \theta = 0, 2\pi \quad (8b)$$

where

$$F(\theta, n) = [c_1 \sin(n\theta/2 + 1) + c_2 \cos(n\theta/2 + 1) + c_3 \sin(n\theta/2 - 1) + c_4 \cos(n\theta/2 - 1)] \quad (9)$$

this implies that

$$F(0, n) = F'(0, n) = F(2\pi, n) = F'(2\pi, n) = 0 \quad (10)$$

From this set of homogeneous equations it can be determined that

$$F(0, n) = 0, F(2\pi, n) = 0 \quad c_2 = -c_4 \quad (11a)$$

$$F'(0, n) = 0, F'(2\pi, n) = 0 \quad c_1 = -\frac{(n-2)}{(n+2)} c_3 \quad (11b)$$

The stress function can then be written in terms of c_3 and c_4 as

$$(r, \theta, n) = r^{n/2+1} \left[c_3 \sin\left(\frac{n\theta}{2} - 1\right) - \frac{n-2}{n+2} \sin\left(\frac{n\theta}{2} + 1\right) + c_4 \left[\cos\left(\frac{n\theta}{2} - 1\right) - \cos\left(\frac{n\theta}{2} + 1\right) \right] \right] \quad (12)$$

To convert this to a more recognizable form a coordinate transform can be performed (Fig. 2)

= -

$$\text{For } n=1, 3, 5, \dots \quad \text{Let } n = 2n-1 \quad n=1, 2, 3 \quad (13)$$

$$\text{For } n=2, 4, 6, \dots \quad \text{Let } n = 2n \quad n=1, 2, 3$$

$$(r, \theta, n) = \sum_{n=1}^{\infty} r^{n+1/2} \left[c_{2n-1} \sin\left(\frac{(n-3/2)(\theta + \theta_0)}{2}\right) - \frac{2n-3}{2n+1} \sin\left(\frac{(n+1/2)(\theta + \theta_0)}{2}\right) + d_{2n-1} \left[\cos\left(\frac{(n-3/2)(\theta + \theta_0)}{2}\right) - \cos\left(\frac{(n+1/2)(\theta + \theta_0)}{2}\right) \right] \right] + \sum_{n=1}^{\infty} r^{n+1} \left[c_{2n} \sin\left(\frac{(n-1)(\theta + \theta_0)}{2}\right) - \frac{2n-2}{2n+2} \sin\left(\frac{(n+1)(\theta + \theta_0)}{2}\right) + d_{2n} \left[\cos\left(\frac{(n-1)(\theta + \theta_0)}{2}\right) - \cos\left(\frac{(n+1)(\theta + \theta_0)}{2}\right) \right] \right] \quad (14)$$

By simplifying the trigonometric relations with the following substitutions:

$$\begin{aligned}
 \sin\left(\left(n - \frac{3}{2}\right)\theta\right) &= (-1)^{n+1} \cos\left(\left(n - \frac{3}{2}\right)\theta\right) & \sin\left((n-1)\theta\right) &= (-1)^{n+1} \sin\left((n-1)\theta\right) \\
 \cos\left(\left(n - \frac{3}{2}\right)\theta\right) &= (-1)^{n+1} \sin\left(\left(n - \frac{3}{2}\right)\theta\right) & \cos\left((n-1)\theta\right) &= (-1)^{n+1} \cos\left((n-1)\theta\right) \\
 \sin\left(\left(n + \frac{1}{2}\right)\theta\right) &= (-1)^{n+1} \cos\left(\left(n + \frac{1}{2}\right)\theta\right) & \sin\left((n+1)\theta\right) &= (-1)^{n+1} \sin\left((n+1)\theta\right) \\
 \cos\left(\left(n + \frac{1}{2}\right)\theta\right) &= (-1)^{n+1} \sin\left(\left(n + \frac{1}{2}\right)\theta\right) & \cos\left((n+1)\theta\right) &= (-1)^{n+1} \cos\left((n+1)\theta\right)
 \end{aligned} \tag{15}$$

the stress function becomes

$$\begin{aligned}
 (r, \theta) = & \sum_{n=1}^{\infty} r^{n+1/2} c_n (-1)^{n+1} \cos\left(\left(n - \frac{3}{2}\right)\theta\right) - \frac{2n-3}{2n+1} (-1)^{n+1} \cos\left(\left(n + \frac{1}{2}\right)\theta\right) \\
 & + d_n \left[(-1)^{n+1} \sin\left(\left(n - \frac{3}{2}\right)\theta\right) - (-1)^{n+1} \sin\left(\left(n + \frac{1}{2}\right)\theta\right) \right] \\
 & + \sum_{n=1}^{\infty} r^{n+1} c_n (-1)^{n+1} \sin\left((n-1)\theta\right) - \frac{2n-2}{2n+2} (-1)^{n+1} \sin\left((n+1)\theta\right) \\
 & + d_n \left[(-1)^{n+1} \cos\left((n-1)\theta\right) - (-1)^{n+1} \cos\left((n+1)\theta\right) \right]
 \end{aligned} \tag{16}$$

Separated into even and odd functions the stress function can be written

$$\begin{aligned}
 o(r, \theta) = & \sum_{n=1}^{\infty} b_{2n-1} (-1)^{n+1} r^{n+1/2} \left[\sin\left(\left(n - \frac{3}{2}\right)\theta\right) - \sin\left(\left(n + \frac{1}{2}\right)\theta\right) \right] \\
 & + \sum_{n=1}^{\infty} b_{2n} (-1)^{n+1} r^{n+1} \left[\sin\left((n-1)\theta\right) - \frac{2n-2}{2n+2} \sin\left((n+1)\theta\right) \right]
 \end{aligned} \tag{17a}$$

$$\begin{aligned}
 e(r, \theta) = & \sum_{n=1}^{\infty} a_{2n-1} (-1)^{n+1} r^{n+1/2} \left[\cos\left(\left(n - \frac{3}{2}\right)\theta\right) - \frac{2n-3}{2n+1} \cos\left(\left(n + \frac{1}{2}\right)\theta\right) \right] \\
 & + \sum_{n=1}^{\infty} a_{2n} (-1)^{n+1} r^{n+1} \left[\cos\left((n-1)\theta\right) - \cos\left((n+1)\theta\right) \right]
 \end{aligned} \tag{17b}$$

The even stress function relates to the symmetric mode I stress intensity distribution where the odd function relates to the antisymmetric mode II stress intensity distribution. Using the odd stress function as an example, the stresses can be derived by first calculating the appropriate derivatives taking into account the change in variables,

$$\begin{aligned} \frac{\sigma}{r} = & \left\{ (-1)^{n+1} (n+1/2) b_{2n-1} r^{n-1/2} [\sin(n-3/2) - \sin(n+1/2)] \right\} \\ & + (-1)^n (n+1) b_{2n} r^n - \sin(n-1) + \frac{2n-2}{2n+2} \sin(n+1) \end{aligned} \quad (18a)$$

$$\begin{aligned} \frac{\sigma}{r^2} = & \left\{ (-1)^{n+1} (n+1/2)(n-1/2) b_{2n-1} r^{n-3/2} [\sin(n-3/2) - \sin(n+1/2)] \right\} \\ & + (-1)^{n+1} n (n+1) b_{2n} r^{n-1} - \sin(n-1) + \frac{2n-2}{2n+2} \sin(n+1) \end{aligned} \quad (18b)$$

$$\begin{aligned} \frac{\sigma}{2} = & (-1)^{n+1} b_{2n-1} r^{n+1/2} - (n-3/2)^2 \sin(n-3/2) + (n+1/2)^2 \frac{2n-3}{2n+1} \sin(n+1/2) \\ & + (-1)^{n+1} b_{2n} r^{n+1} - (n-1)^2 \sin(n-1) + (n+1)^2 \frac{2n-2}{2n+2} \sin(n+1) \end{aligned} \quad (18c)$$

Sparing the algebraic detail the first stress invariant ($\sigma_r + \sigma_\theta$) simplifies to

$$\sigma_1 = \sum_{n=1} (-1)^{n+1} (4n-2) b_{2n-1} r^{n-3/2} \sin n - \frac{3}{2} + 4 \sum_{n=1} (-1)^{n+1} b_{2n} n r^{n-1} \sin(n-1) \quad (19a)$$

Notice that the $\sin(n+1/2)$ and the $\sin(n+1)$ terms completely cancel. A similar derivation can be performed to determine the first stress invariant for the even stress functions.

$$\sigma_1 = \sum_{n=1} (-1)^{n+1} (4n-2) a_{2n-1} r^{n-3/2} \cos n - \frac{3}{2} + 4 \sum_{n=1} (-1)^{n+1} a_{2n} n r^{n-1} \cos(n-1) \quad (19b)$$

Exercising poetic license and redefining **a** and **b** to absorb all constants and defining the leading terms to be compatible with the common definition of stress intensity factors, the complete stress state in terms of the first stress invariant is

$$\sigma_1 = K_I \sqrt{\frac{2}{r}} \cos(\theta/2) + K_{II} \sqrt{\frac{2}{r}} \sin(\theta/2) + A_0 + \sum_{n=1} a_n r^{n/2} \cos(n\theta/2) + \sum_{n=1} b_n r^{n/2} \sin(n\theta/2) \quad (20)$$

4.0 Fitting Algorithm

The analytical solution describes all the possible stress states that could occur within a zone immediately surrounding a crack tip irregardless of the geometric details outside of the area (Fig. 3).

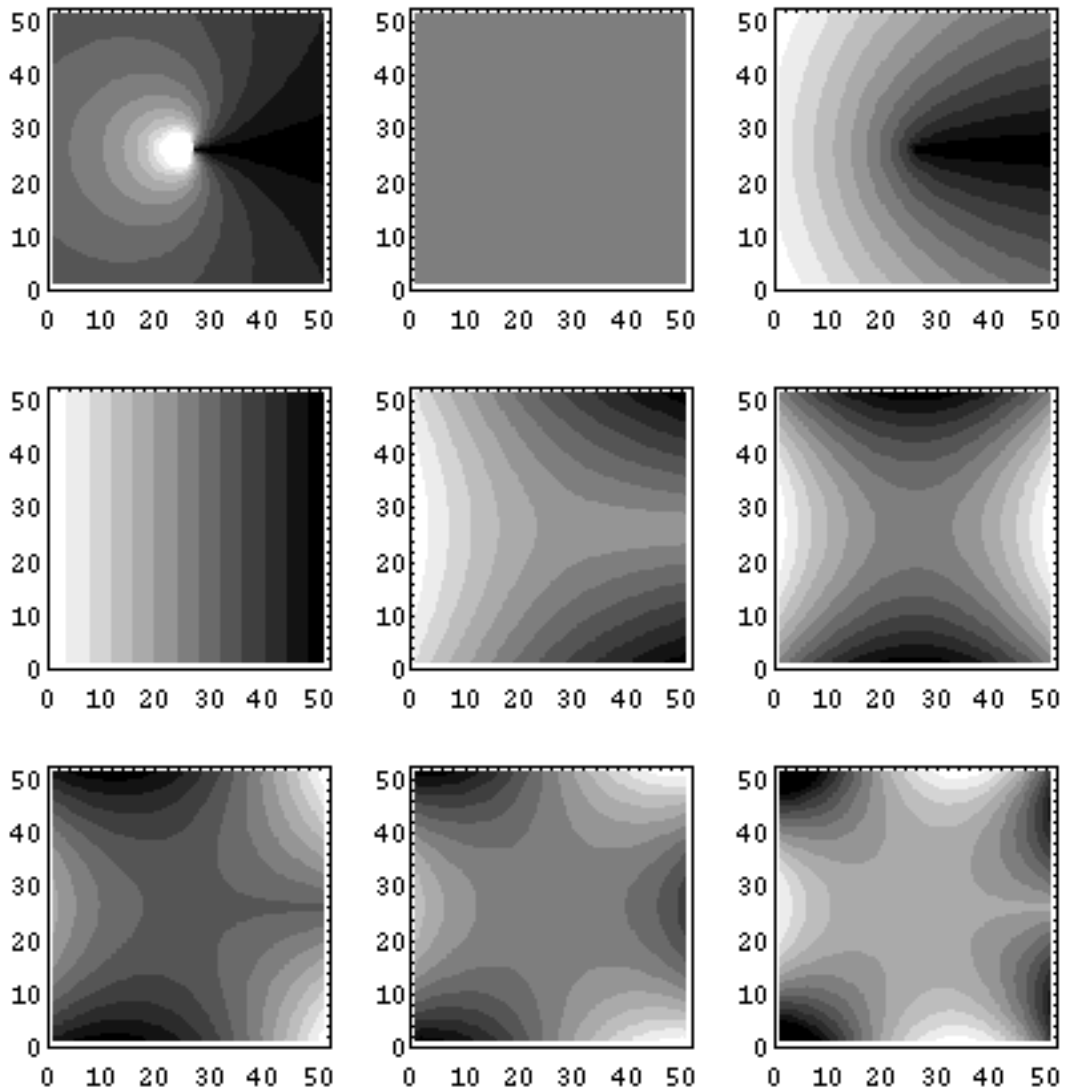


Fig. 3 Even modes of analytical fits, K_I , A_0 , $n=1, 7$

A fit window is established to designate the data to be used in the fit (Fig. 4). Although the fit window is not necessarily circular or concentric about the crack tip a sufficient number of stress terms will describe an arbitrary planer stress state about the crack tip. An exclusion zone is established in the immediate area of the crack tip to eliminate the use of high stress-gradient data which can be tainted by heat conduction or nonlinear material behavior. A fully elastic body loaded at an adiabatic frequency can be phased in so that all the oscillating thermal signal is perfectly synchronized to the loading. The in-phase image resulting from the lock-in electronics represents the signed amplitude of the thermal oscillations and the out-of-phase image should be null. Any material experiencing nonlinear behavior or thermal conduction will show a deviation in phase; therefore, the radius of the exclusion zone can be determined by examining the out-of-phase image or the actual phase image. To understand the compromise that must be made between algorithm application expediency, stress resolution and the generality of the model stress distribution a closer examination of the fit algorithm is offered.

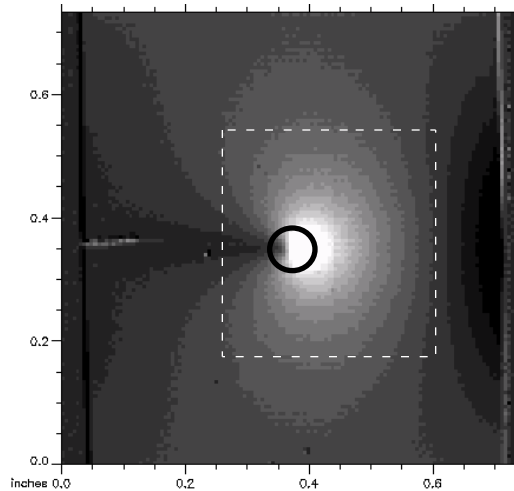


Fig 4. Data set with square fit window and circular exclusion zone

4.1 Least Squares Fitting

Once the appropriate fit window is established, a matrix form of multiple regression least squares fitting is performed. The individual model stress distributions can be viewed as elements of a basis that must span all potential stress distributions. A specific stress image can be constructed as described in the following relationship:

$$\{S\} = \begin{bmatrix} T_{KI} & T_{KII} & A_0 & A_1 & B_2 & \dots & A_n & B_n \end{bmatrix} \begin{matrix} K_I \\ K_{II} \\ a_0 \\ a_1 \\ b_2 \\ \dots \\ a_n \\ b_n \end{matrix} \quad (21)$$

Where the elements of the basis are defined in eq. 20 so that T_{KI} and T_{KII} describe the stress singularities associated with the stress intensity factors, A_0 is a uniform value a_0 , and A_n , B_n describe all other terms. In the context of these arguments, the two dimensional data and stress terms are considered to be reorganized in one dimensional vectors. Equation 21 can be written more simply as

$$\{S\} = [Q]\{C\} \quad (22)$$

The least squares algorithm applied to eq. 22 yields

$$[Q]^T\{S\} = [Q]^T[Q]\{C\} \quad (23)$$

To simplify the least square algorithm the basis is orthogonalized and normalized over the fit window so that

$$[Q']^T[Q'] = I \quad (24)$$

this simplifies the solution of eq. 23 to

$$[Q']^T\{S\} = \{C'\} \quad (25)$$

The orthonormalization allows for rapid application and reapplication of the fit. The orthogonalization process is ordered in such a manner so that the solution matrix C' yields K_I directly; however, a history of the orthogonalization must be maintained in order to extract K_{II} from the solutions vector.

4.2 Stress and Tip Location Resolution

The signal to noise ratio for stress intensity measurement is related to the root of the total points used in the fit window. If a system resolution of 5mK in a 10 second scan is possible and a fit window utilizing 400 data points is used then a final intensity resolution of 0.25mK is possible.

The crack tip location is optimized automatically by a search routine that reapplies the fit in the vicinity of the user estimated crack tip. The tip search algorithm is essential to crack tip following. The actual location of the tip can be interpolated to a partial pixel size. For example, a scan area of 50mm x 50mm the crack tip location is accurate to approximately 0.20mm. This resolution can be improved on as the scan area is reduced. Scans as small as 12.8mm x 12.8mm are routinely captured.

5.0 Results

5.1 Mode 1

A series of Mode I tests were performed to demonstrate the accuracy of the technology. Pin-gripped specimens with crack length ratios of 0.225, 0.33 and 0.5 were tested (Fig.5).

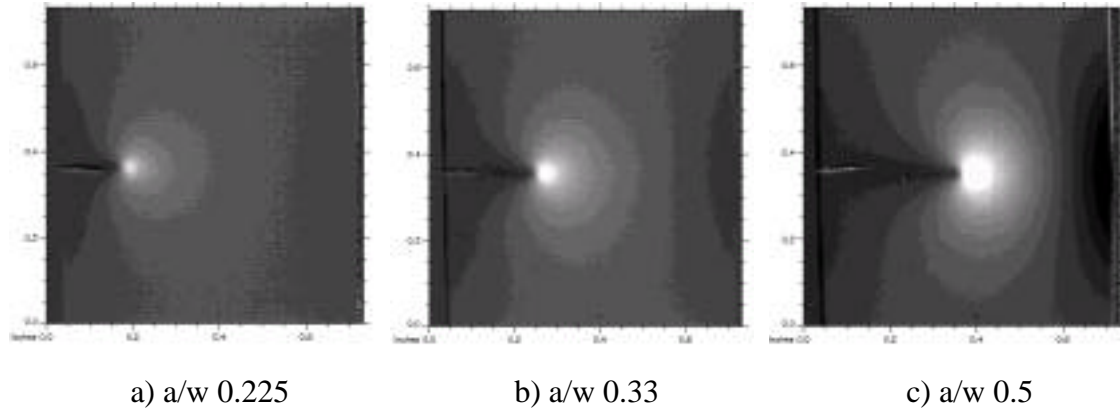


Fig. 5 Mode I data sets

The specimens were fabricated from 1.6mm thick machine steel. The image acquisition time was 60 seconds for these example images. This lengthy acquisition time is not necessary to make accurate measurements for crack growth work. Stress images can be acquired in just a few load cycles. Analytical solutions in terms of the normalized load for this specimen are readily available and are plotted with measured values in Fig. 6. As a test three different loads were used for the same geometry. The three measurements of the dimensionless intensity factor Y do not deviate more than 3%.

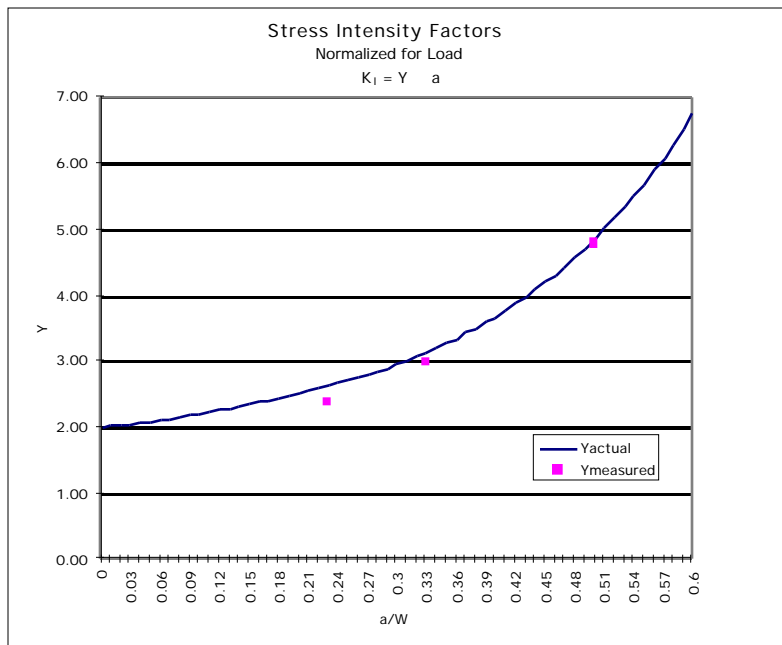


Fig. 6 Mode 1 stress intensity factors, analytical and measured

5.2 Mixed Mode

A mixed mode specimen was manufactured to demonstrate the abilities of TSA to separate the ratio of mode I and mode II (Fig. 7). The analytical solutions for the stress intensity factors versus measured results are described in Table 1.

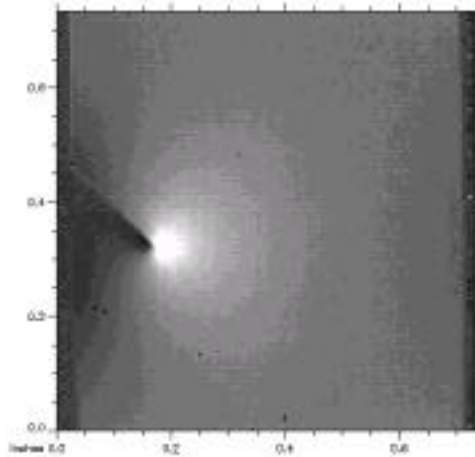


Fig. 7 Mixed mode data

a/w	Y _{actual}	Y _{measured}	% Error
0.225	2.64	2.4	9.09
0.33	3.15	3	4.79
0.5	4.86	4.8	1.23
mixed K _I , K _{II}	1.53, 0.79	1.61, 0.96	-5.02, -20.8

Table 1. Mixed mode stress intensity measurements

6.0 Conclusion

It has been demonstrated that TSA is capable of making accurate non-contacting mixed mode stress intensity measurements. Limited data has been collected on mixed mode cracks; improvements in this area are expected. TSA has been demonstrated to work accurately at temperatures exceeding 1000°C in hostile environments. Efforts are underway to apply this damage evolution work to high-temperature situations. Plasticity and other material behaviors will be considered further. Even though great effort can be taken to match analytical solutions with experimental data, accounting for all nonlinearities and material properties, the technique as it stands can be used to predict the likelihood of failure if the measurements are consistent for a given material and thickness over a range of load conditions. Future efforts of this work will test the damage evaluation system's ability to use fracture mechanics arguments to predict actual failure. This will be the true test of the usefulness of this technology.